Flavon magnetobaryogenesis

Fatemeh Elahi[1,2,*] and Shiva Rostam Zadeh[1,†]

[1]*School of Particles and Accelerators, Institute for Research in Fundamental Sciences IPM, Tehran 19 56 83 66 81, Iran*

[2]*PRISMA$^+$ Cluster of Excellence & Mainz Institute for Theoretical Physics, Johannes Gutenberg-Universität Mainz, 55099 Mainz, Germany*

(Received 16 August 2020; accepted 12 October 2020; published 16 November 2020)

In this paper, we explore the evolution of baryon asymmetry as well as the hypermagnetic field in the early universe with an assumption that the flavon of the Froggatt-Nielsen carries an asymmetry. Through the decay of the flavon to Standard Model fermions, this asymmetry is transferred to fermions, where the right-handed electron keeps its asymmetry while its Yukawa interaction is out of thermal equilibrium. Through the existence of the flavon, we can ensure that the freezing-in temperature of the right-handed electron is closer to the electroweak phase transition than the Standard cosmology scenario. With this trick, the asymmetry in the right-handed electron is saved for a longer time. Moreover, the injection of the asymmetry to the right-handed electron is gradual, which helps the preservation of the asymmetry in the right-handed sector significantly. Due to the intimate relationship between fermion number violation and the helicity of the hypermagnetic field, some of the asymmetry is used to amplify the hypermagnetic field which itself helps to preserve the remnant asymmetry through keeping the Yukawa processes out of thermal equilibrium. We find the sweet region of the parameter space that can produce the right asymmetry in the baryons while generating a large hypermagnetic field by the time of the electroweak phase transition.

DOI: 10.1103/PhysRevD.102.096018

I. INTRODUCTION

One of the most intriguing questions of particle physics is the observation of matter-antimatter asymmetry. The observed asymmetry of the baryons is

$$\eta_B \equiv \frac{n_B - n_{\bar{B}}}{s} \simeq 8.5 \times 10^{-11}, \tag{1}$$

with $s = 2\pi^2 g_\star T^3/45$ being the entropy density. The value of η_B has been obtained by two orthogonal methods, one from the big bang nucleosynthesis measurements [1] and another one from the Planck data [2], and they match miraculously. If the universe had started with an equal number of baryons as antibaryons, three necessary and sufficient conditions known as Sakharov conditions are needed to generate a baryonic asymmetry: (1) Baryon number violation, (2) C and CP violation, and (3) out of thermal equilibrium process [3]. To explain the observed baryon asymmetry of the universe, physics beyond the Standard Model (SM) and new degrees of freedom are needed (e.g., [4,5]). Furthermore, it has been shown that baryon number violation is highly influenced by the presence of a hypermagnetic field [6–18]. That is because in the Standard Model (SM), baryon number violation is proportional to $E_Y \cdot B_Y$, where E_Y and B_Y are the hypercharge electric and magnetic fields, respectively.

Interestingly, there are some questions in the observations of widespread large scale magnetic fields in the Universe as well. Large scale magnetic fields in causally disconnect patches have been observed to have similar amplitudes [19–21]. Even though part of the community believes that the origin of these magnetic fields is some astrophysical activities due to late post-recombination physics, some cosmologists insist that these observations roots in the early Universe. There exist different scenarios which try to explain the origin and the evolution of these cosmic magnetic fields which are referred to as magnetogenesis scenarios [6,7,13,14,22–35]. The evolution of the magnetic fields is not rigorously understood; however simple conservative estimates indicate that to justify the current magnetic fields, we need to have magnetic fields with amplitudes about 10^{20} G by the electroweak phase transition (EWPT) [7,12–14,36–38]. It is worth emphasizing that the quoted value is a rough estimate since there are numerous nonlinear effects before and after the EWPT that have not been considered in this estimation.

*felahi@ipm.ir
†sh_rostamzadeh@ipm.ir

In this paper, we are interested in scenarios where the initial seed of the hypermagnetic field amplitude (HMFA) is small, and through the existence of baryonic asymmetry, we get a large value of HMFA ($\sim 10^{20}$ G) by the time of EWPT. In Ref. [9], however, the authors have shown that in the standard cosmology (SC), this is rather impossible, even if we start with a large baryonic asymmetry. Therefore, we need to consider alternatives in the nonstandard cosmology.

To succeed in our mission, on the one hand, we need a mechanism that generates a large baryonic asymmetry that can be used to amplify a small seed of hypermagnetic field; on the other hand, we need to control the effect of the sphalerons—either by changing the Hubble rate such that the freeze-in[1] of the right-handed electron occurs closer to the EWPT and/or by injection the asymmetry into right-handed electron slowly.

The importance of the right-handed electron is because of the following: If we insist on having the constraint $B - L = 0$ and we have some initial asymmetry in the right-handed electron, then we must have some asymmetry in the baryonic sector as well. Right-handed electrons at high temperatures are not in thermal equilibrium and therefore cannot lose their asymmetry. However, once their Yukawa interaction's rate gets higher than the Hubble rate, then the asymmetry in the right-handed electron can be transferred into a left-handed electron and electron neutrino, and then weak sphalerons can wash out the asymmetry—eating the asymmetry preserving $B - L$ until it becomes zero. Before the EWPT, the rate of weak sphalerons is proportional to T^4, but then after the EWPT, their rate becomes increasingly more suppressed. Therefore, the rate of change in baryon asymmetry is more efficient before the EWPT. In the standard cosmology, the difference between the freeze-in temperature of right-handed electron, $T_R \simeq 10^5$ GeV, and the temperature at which EWPT occurs (T_{EW}) is large enough that the weak sphalerons have enough time to wash out the asymmetry. To avoid this problem, one solution is to change the cosmological evolution.

Recently, Chen *et al.* [39] discussed the generation of baryon asymmetry through the decay of the flavon. In this paper, the flavon dominates the energy density of the universe and causes the freeze-in of the right-handed electron to delay. Their scenario is motivated because the flavon of the Froggatt Nielsen (FN) is theoretically motivated to justify the hierarchy of fermion masses [40–42]. The paper [39] has an obvious merit in that it explains two problems with a single theory. In this paper, we would like to be even more ambitious and find the region of the parameter space that can solve the magnetogensis as well. We find that only a small region of the parameter space can give satisfactory results, and that is with the assumption that the flavon only couples to the first generation of fermions. This way, the branching ratio of the flavon to the electron is more significant and thus more asymmetry can be transferred into the fermionic sector. Since the masses of the first generation are the most troublesome compared with the electroweak scale, we insist that this assumption is justifiable.

Our results give the most desirable outcome when the cutoff of the theory is about $10^{7.5}$ GeV, and the mass of the flavon is nearly 15 TeV. The initial comoving wave number of the hyermagnetic field should also be about $0.5 \times 10^{-7} \times T_\star$, where $T_\star$ is when the flavon starts dominating.

The organization of the paper is as follows: In Sec. II, we explain the FN mechanism and the couplings of the flavon with fermions. The nature of the FN symmetry as well as the evolution of the flavon in the early universe are discussed in Secs. II A and II B, respectively. Section III is devoted to the evolution of the hypermagnetic field and Sec. IV discusses the Boltzmann equation of the right-handed electron in the presence of a flavon, sphaleron, and a nonzero small seed of the hypermagnetic field. In Sec. V, we do a numerical study of the coupled Boltzmann equations. First, we discuss one benchmark in great detail, and then we scan through the parameter space and find the desired region. The concluding remarks are presented in Sec. VI.

II. FLAVON MODEL

The Froggatt-Nielsen (FN) mechanism is a proposal to reproduce the mass hierarchy among the Standard Model (SM) fermions with $O(1)$ Yukawa couplings. The solution it proposes is charging the fermions under a new symmetry such that the lighter fermions have a larger charge. The charges of the fermions causes their Yukawa interactions to be modified. That is their Yukawa interactions at low energies become

$$\mathcal{L}_{\mathrm{Yuk}} \supset y^f_{ij} \left(\frac{S_0}{\Lambda}\right)^{n_{ij}} \bar{f}_{L_i} \phi f_{R_j}, \tag{2}$$

where ϕ represents the Higgs, and $f_{L,R}$ are the SM left-handed and right-handed fermions, respectively. The indices i, j represent the fermion's generations, and n_{ij} is related to the FN charges of fermions. The complex scalar S_0, known as flavon, has a charge of -1 under the FN symmetry, and it is used to cancel the charges of the fermions in the Yukawa interactions. In this setup, Higgs does not have any FN charges. The cutoff scale Λ represents the mass of some vectorlike fermions at UV scales. Once S_0 acquires a vacuum expectation value (vev), the FN symmetry spontaneously breaks. After the FN spontaneous symmetry breaking (SSB), S_0 obtains a dynamical part S and a constant part v_s: $S_0 \to S + v_S$. The masses of fermions are the result of both electroweak

[1]The temperature at which the right-handed electron comes into thermal equilibrium.

SSB *and* FN SSB,[2] and are proportional to $y_{ij}(\frac{v_S}{\Lambda})^{n_{ij}} v_\phi$, i.e., the SM Yukawa couplings of fermions are $y_{ij}(\frac{v_S}{\Lambda})^{n_{ij}}$. Knowing the fermion masses and their FN charges, $\epsilon \equiv v_S/\Lambda$ can be estimated, and in the most minimalistic scenario, it is approximately 0.2. The purpose[3] of the FN mechanism is to make the y_{ij} in Eq. (2) natural, O(1).

We consider a scenario where the FN SSB occurs much earlier than the EWPT, and thus it is important to comment on the coupling of the dynamical field S with $\bar{f}_{L_i} f_{R_j} \phi$. We use the notation where this coupling is g_{ij}/Λ, with

$$g_{ij} \equiv y_{ij}^f n_{ij} \epsilon^{n_{ij}-1}. \tag{3}$$

Furthermore, we focus on the case where only the first generation is charged under the FN symmetry.[4] This is justified because the first-generation has the smallest masses in the SM. Specifically, we will take the charges of the first generation as the following [43]

$$Q_{\rm FN}(\bar{Q}_1, u_1, d_1, \bar{L}_1, e_1) = (3, 5, 4, 5, 4), \tag{4}$$

which using the definition $n_F = n_{\bar{F}_L} + n_{F_R}$ leads to

$$n_e = 9 \qquad n_u = 8 \qquad n_d = 7. \tag{5}$$

A. The nature of the FN symmetry and the generation of flavon asymmetry

Thus far, we have not commented on the nature of the FN symmetry. In the following, we will discuss what kind of symmetries are suitable. In general, the FN symmetry can be global/local and continuous/discrete. Given that the FN symmetry is severely anomalous, we focus on the global case. As a result of SSB of continuous global symmetry, a massless Goldstone boson emerges; a consequence that is strongly disfavored by CMB [44–46]. To avoid this problem, we can assume the FN symmetry is discrete, $\mathbb{Z}_N$ [47], where we take $N = 20$ to make sure the charges of light fermions are well defined. Even though the SSB of a discrete symmetry leads to the production of domain walls in the early Universe, the lack of observation of domain walls so far can be cosmologically justified (see Refs. [48–51] for more information). After the FN SSB, both the real and the imaginary components of S gain different nonzero masses. However, as argued in Ref. [39], one could start with more complex fields and the flavon can be defined as a complex linear combination of these fields with the same mass. The sameness of the mass of these degrees of freedom can be protected by a symmetry such as a custodial symmetry [52,53]. Defining S as a complex linear combination of the scalars means that S can carry some initial asymmetry (e.g., through Affleck-Dine mechanism [5,39]).

It should be noted that the non-renormalizable interactions of the flavon, e.g.,

$$V(S) = \frac{\kappa}{\Lambda^{N-4}} S^N + \frac{\kappa'}{\Lambda^{N-4}} S^{*N} + V'(SS^*), \tag{6}$$

with $\kappa^* \neq \kappa'$, are responsible for the generation of flavon asymmetry [54]. Thereby, their effect is more relevant at high temperatures, when the suppression of T/Λ is smaller; but they are irrelevant at lower temperatures. Here, we assume a positive asymmetry in the flavon is generated at high temperatures.

B. The cosmology of the flavon

In our scenario, we need the flavon to have a large asymmetry at high temperatures. This asymmetry should be conserved until the flavon starts its coherent oscillation. During this epoch, the flavon decays to fermions through $S \to f_{L_1} f_{R_1} \phi$, and its asymmetry penetrates to the fermionic sector. In the following, we will discuss each of these steps in greater detail.

A weakly interacting scalar field goes through coherent oscillation for a period of $H \lesssim m_S$. That is for temperatures below $\sqrt{M_H m_S}$, where $M_H = M_{\rm Pl}/(1.66\sqrt{g_*}) \simeq 1.4 \times 10^{17}$ GeV is the reduced Planck mass and m_S is the flavon mass. It is worth saying that lighter flavons have larger amplitudes of oscillation and thus enjoys higher yield [47].

In order to have a successful coherent oscillation, we must make sure that the production of the flavon is out of equilibrium [47]. Thereby, we require

$$n\langle\sigma v\rangle_{f_{L_1} f_{R_1} \to SH} \simeq \zeta(3) \frac{T^3}{4\pi^3} \frac{\sum_{f=e,u,d} |g_f|^2}{\Lambda^2} < H. \tag{7}$$

This condition ensures that excited states of flavons, which would have messed up their coherency, do not get produced. Let us define the temperature at which the rate of the flavon production equals to Hubble rate as T_M:

$$T_M(\Lambda) \equiv \frac{4\pi^3 \Lambda^2}{\zeta(3) M_H \sum_{f=e,u,d} |g_f|^2}. \tag{8}$$

In order to obtain the above equation, we have used the effective field theory (EFT) approach, and thus the maximum temperature of the Universe ($T_{\rm max}$) must be smaller than Λ. Therefore, we require $T_{\rm max}(\Lambda) \equiv \min[T_M(\Lambda), \Lambda]$.

[2]We assume the electroweak SSB to occur around $T_{\rm EW} \simeq 160$ GeV. The FN SSB is expected to be at much higher temperatures, but its value is a free parameter that can be tuned.

[3]It is important to mention that fermions, unlike Higgs, do not suffer from untamed quantum corrections. That is the radiative correction to their mass is always proportional to v_h and thus it is finite.

[4]Note that we do not have any off-diagonal entry in the couplings of the flavon with the SM fermions. In other words, the couplings of fermions with the flavon in the interaction basis are the same as the mass basis.

During the coherent oscillation, the flavon redshifts like cold matter (i.e., $\rho_S \propto a^3$). Consequently, at some temperature $T_\star$, the energy density of the flavon equals that of the radiation: $\rho_S|_{T_\star} = \rho_{\rm rad}|_{T_\star}$. For $T < T_\star$, ρ_S dominates the energy density of the Universe, and thus the Hubble rate gets modified. During this epoch, the flavon decays to $ff\phi$ which contributes to the radiation of the universe, increasing $\rho_{\rm rad}$, and eventually leading to the termination of the matter-domination. The evolution equations of ρ_S and $\rho_{\rm rad}$ are as follows [39]:

$$\begin{aligned} \dot{\rho}_S + 3H\rho_S &= -\Gamma_S \rho_S \\ \dot{\rho}_{\rm rad} + 4H\rho_{\rm rad} &= \Gamma_S \rho_S, \end{aligned} \tag{9}$$

with

$$\Gamma_S = \frac{\sum_{f=e,u,d}|g_f|^2}{64\pi^3\epsilon^2}\frac{m_S^3}{\Lambda^2} \tag{10}$$

being the total decay of the flavon ($S \to f_{L_1} f_{R_1} H$), and

$$H = \sqrt{\frac{8\pi}{3M_{\rm Pl}^2}(\rho_S + \rho_{\rm rad})},$$

being the Hubble rate.

The analytical approximate solutions of Eqs. (9) for the time interval $t_\star < t < \Gamma_S^{-1}$ are the following [55]:

$$\begin{aligned} \rho_S^a(t) &\simeq \frac{M_{\rm Pl}^2}{6\pi t^2} e^{-\Gamma_S t} \\ \rho_{\rm rad}^a(t) &\simeq \frac{M_{\rm Pl}^2 t_\star^{2/3}}{6\pi t^{8/3}} + \frac{\Gamma_S M_{\rm Pl}^2}{10\pi t}, \end{aligned} \tag{11}$$

where $t_\star$ is the time that corresponds to $T_\star$. To convert between temperature and time, we use the definition of the temperature, which is

$$T = \left(\frac{\rho_{\rm rad}(t)}{\frac{\pi^2}{30} g_\star}\right)^{1/4}. \tag{12}$$

In order to obtain $t_\star$ for a given $T_\star$, we simply plug in the analytical solution, $\rho_{\rm rad}^a(t_\star)$ into the above equation, and solve for $t_\star$. Equations (11) are also used to get $\rho_{S({\rm rad})}(t_\star) = \rho_{S({\rm rad})}^a(t_\star)$, which are needed as the initial conditions for solving Eqs. (9) numerically. Other than the aforementioned tasks, we do not rely on the analytical solutions [Eqs. (11)] anymore. The numerical solution of ρ_S and $\rho_{\rm rad}$ as a function of temperature, assuming $T_\star = T_{\rm max}(\Lambda = 10^8\ {\rm GeV})$, are shown in Fig. 1—upper panel. The lower panel compares the time-temperature conversion in the SC and our scenario which includes an intermediate matter domination (nonstandard cosmology).

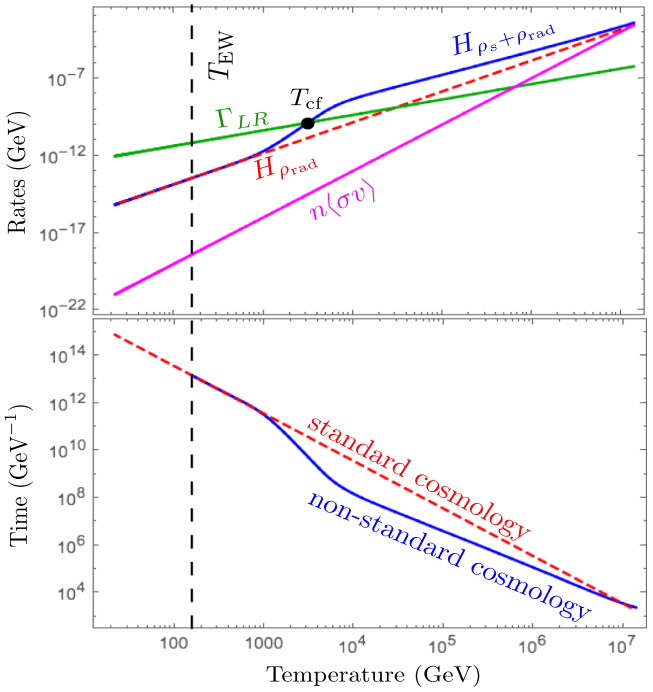

FIG. 1. The Hubble rates both in our scenario $H_{\rho_S+\rho_{\rm rad}}$ (shown in solid blue) and in the standard cosmology $H_{\rho_{\rm rad}}$ (dashed red), as well as the rate of electron Yukawa interaction Γ_{LR} (solid green) are shown in the upper panel. As the plot demonstrates, $T_{\rm cf}$ is much closer to the EW temperature in the presence of a flavon than the standard cosmology. For the demonstration, we have also shown the rate of production of flavon $n\langle\sigma v\rangle$ (in magenta) to ensure that the flavon is indeed out of equilibrium and thus goes through coherent oscillation and redshifts like matter. The relation between time and temperature in the nonstandard (solid blue) and standard (dashed red) cosmology is shown in the lower panel and it demonstrates once the flavon decays, we are back to standard cosmology. This plot is with the assumption that $T_\star = 1.4 \times 10^6$ GeV.

As it is apparent in Eq. (2), the flavon interactions with SM particles respect B and L symmetries, and therefore the $B - L$ symmetry, that is respected in the framework of the SM as well. As a result of the flavon and antiflavon decaying to SM fermions and antifermions, the flavon-antiflavon asymmetry is transferred to left-right asymmetry in the SM content. The left-right asymmetry produced in the quark sector is washed out immediately by the strong sphalerons. However, in the leptonic sector, the produced asymmetry in the right-handed electron is preserved above a critical temperature.[5] Therefore, the weak sphalerons, which are only active before the EWPT and act only on left-handed particles, partially convert the asymmetry of left-handed leptons into a baryon (B) asymmetry [56].

[5]Soon it will be clarified that this is the temperature at which the chirality flip rate of the electron becomes equal to the Hubble rate.

Consequently, we gain a simultaneous asymmetry in the quark and lepton sectors. Indeed, weak sphalerons tend to wash out the asymmetry of these two sectors. However, the washout process is successful if and only if all of the Yukawa interactions are in thermal equilibrium [8,55–61]. The rate of the Yukawa interactions is proportional to $y_f^2 T$, where y_f is their SM Yukawa coupling. Since electrons have a small Yukawa coupling, they are the last fermions[6] that enter thermal equilibrium, and thus the action of weak sphalerons is limited by electron's chirality flip process [57–59]. Specifically, it is the right-handed electron that plays a key role in preserving the asymmetries.

Due to the importance of the chirality flip of the right-handed electron, its rate has been extensively studied, and the most recent calculation of it is [61,62]:

$$\Gamma_{LR} \simeq 10^{-2} y_e^2 T. \tag{13}$$

Let us define the temperature at which the chirality flip of the right-handed electron process goes to equilibrium as $T_{\rm cf} \equiv T|_{\Gamma_{LR}\sim H}$. In the SC, $T_{\rm cf}$ is about (10–100) TeV, as can be seen in Fig. 1.[7] Even though the asymmetries are preserved up to this temperature, it has been shown that below $T_{\rm cf}$ the weak sphalerons still have enough time to wash out the asymmetries due to their high rates [57–59]. In this scenario, however, the presence of the flavon may change the story [39], because

(i) it brings $T_{\rm cf}$ relatively closer to $T_{\rm EW}$, and
(ii) it transfers the asymmetry to the fermionic sector *gradually*.[8]

In this project, we are not only interested in acquiring the right baryonic asymmetry of the Universe, but also we want the asymmetries to amplify a small seed of the hypermagnetic field to amplitudes as large as 10^{20} G at the onset of the EWPT.[9] It has been argued that a hypermagnetic field with this amplitude at $T_{\rm EW}$ can lead to the observed magnetic fields as large as $10^{-17} - 10^{-15}$ G observed in the intergalactic medium (IGM). Thereby, in this paper, we are interested in the region of the parameter space that yields

$$\begin{aligned} \eta_B(T_{\rm EW}) &\simeq 8.5 \times 10^{-11} \\ B_Y(T_{\rm EW}) &\gtrsim 10^{19}\ \text{G}. \end{aligned} \tag{14}$$

Before the EWPT, the evolution of hypermagnetic fields and the asymmetries are strongly intertwined through the Abelian anomaly ($\partial_\mu J^\mu_{B,L} \propto \vec{E}_Y \cdot \vec{B}_Y$) and chiral magnetic effect (CME) [9,16,17,63–68].[10] These effects, together, ensure the conversion of the asymmetries to the helicity of hypermagnetic fields, and vice versa. However, it has been shown that in the framework of the SM and the presence of the weak sphalerons, the initial asymmetries are rapidly washed out and no growth of the hypermagnetic field happens [9]. Indeed, the growth can happen if the asymmetry is somehow preserved for a longer time compared to SC [9]; a task that is achievable in our model through the flavon.[11] In the following section, we will look at the evolution equations of the hypermagnetic fields.

III. ANOMALOUS MAGNETOHYDRODYNAMICS

In the static limit, the effective action of the soft $U(1)_Y$ gauge fields can be derived via the method of dimensional reduction [64–66]. The corresponding Lagrangian describing the dynamics of these fields at finite fermionic density in the Minkowski spacetime is the following [14,17,64,66]:

$$\mathcal{L} = -\frac{1}{4} Y_{\mu\nu} Y^{\mu\nu} - J^\mu_Y Y_\mu - c'_E \frac{\alpha'}{8\pi} (2Y \cdot B_Y), \tag{15}$$

where $\alpha' \equiv g'^2/4\pi \simeq 0.01$ is the fine structure constant of the hypercharge interaction. In Eq. (15), the first term is the kinetic term of the hypercharge field, J_Y is the Ohmic current, and the last contribution is related to the Chern-Simons term, which leads to the CME [64]. The Chern-Simons coefficient, c'_E, can be written as [17,64]

$$c'_E = \sum_{i=1}^{n_G} \left[-2\mu_{R_i} + \mu_{L_i} - \frac{2}{3}\mu_{d_{R_i}} - \frac{8}{3}\mu_{u_{R_i}} + \frac{1}{3}\mu_{Q_i} \right], \tag{16}$$

where the μ's are the chemical potentials of various chiral fields, and n_G is the number of generations. Let us make the simplifying assumption that all Yukawa interactions, other than that of the electron, are in thermal equilibrium. Thereby, we can obtain all of the chemical potentials in terms of the chemical potential of the right-handed electron by requiring $B/3 - L_i$ (with i being the generation index)

[6] Here, we consider that the neutrinos are massless such as in the SM.

[7] The intersection of the dashed red line and solid green line in the upper panel.

[8] The authors of Ref. [39] considered the decay of the flavon to tau and electron, which leads to a much larger decay width of the flavon compared to that of our scenario. Since the gradual decay of the flavon is more important for our scenario, we considered the decay of the flavon only to the first generation of fermions.

[9] Here we neglect the possible change of the baryonic asymmetry during EWPT.

[10] The CME is the generation of electric field parallel to an external magnetic field induced due to the imbalance of the chirality in the plasma. This effect was first derived by Vilenkin [63]; then it was found to be important in the context of the heavy-ion collision, where the name of the phenomenon was also given(see Refs. [69–71] and references therein).

[11] The arising hypermagnetic field, can in return, push the Yukawa interactions out of equilibrium, assisting the preservation of the asymmetry. The deviation of the Yukawa interactions from equilibrium is highly correlated with their Yukawa rate: the slower the rate, the larger the deviation from equilibrium. Therefore, the effect of the hypermagnetic field is particularly important for the chirality flip of the electrons [9].

conservation as well as the hypercharge neutrality in the plasma. As a result, c'_E can be reduced to $c'_E = -99/37\mu_{e_R}$. Furthermore, one important chemical potential that has observational significance is $\mu_B = \sum_{i=1}^{n_G}[2\mu_{Q_i} + \mu_{u_{R_i}} + \mu_{d_{R_i}}]$. Using the aforementioned simplifying assumptions and conservation laws, we obtain $\mu_B = \frac{198}{481}\mu_{e_R}$ [9,39].

Since we are interested in studying the evolution equation of the hypermagnetic field in the early Universe, we must consider the Friedman-Robertson-Walker (FRW) metric. Therefore, the Lagrangian in Eq. (15) will be slightly modified (see Appendix A in Ref. [72]), and the resulting AMHD equations in the curved spacetime become the following:

$$\frac{1}{a}\vec{\nabla}\cdot\vec{E}_Y = 0, \qquad \frac{1}{a}\vec{\nabla}\cdot\vec{B}_Y = 0 \tag{17}$$

$$\partial_t\vec{B}_Y + 2H\vec{B}_Y = -\frac{1}{a}\vec{\nabla}\times\vec{E}_Y \tag{18}$$

$$\vec{J}_{\rm Ohm} = \sigma(\vec{E}_Y + \vec{v}\times\vec{B}_Y) \tag{19}$$

$$\vec{J}_{\rm cm} = -\frac{\alpha'}{2\pi}c'_E\vec{B}_Y \tag{20}$$

$$\vec{J}_{\rm Ohm} + \vec{J}_{\rm cm} = \frac{1}{a}\vec{\nabla}\times\vec{B}_Y - (\partial_t\vec{E}_Y + 2H\vec{E}_Y), \tag{21}$$

where $\sigma \simeq 100T$ is the electrical hyperconductivity of the plasma, $H = \dot{a}/a$ is the Hubble parameter, a is the scale factor, and the currents $\vec{J}_{\rm Ohm}$ and $\vec{J}_{\rm cm}$ are the Ohmic and chiral magnetic currents, respectively. The latter current, which is in the direction of the hypermagnetic field, comes from the Chern-Simons term and promotes the ordinary magnetohydrodynamics equations to anomalous magnetohydrodynamics (AMHD) equations. The terms containing the Hubble parameter H are related to the expansion of the Universe. Using Eqs. (21) and (19) and neglecting the displacement current $(\partial_t\vec{E}_Y + 2H\vec{E}_Y)$ in the lab frame, the hyperelectric field will be obtained as

$$\vec{E}_Y = \frac{1}{a\sigma}\vec{\nabla}\times\vec{B}_Y + \frac{\alpha'}{2\pi\sigma}c'_E\vec{B}_Y - \vec{v}\times\vec{B}_Y. \tag{22}$$

In the above equation, we can neglect the last term containing the velocity of the plasma. That is because the correlation distance of the hypermagnetic field is much larger than the length scale of the variation of the bulk velocity. Therefore, the hypercharge infrared modes are practically unaffected by the plasma velocity [11].

Replacing Eq. (22) in Eq. (18), we can solve for the evolution equation of the hypermagnetic field:

$$\partial_t\vec{B}_Y + 2H\vec{B}_Y = \frac{1}{a^2\sigma}\nabla^2\vec{B}_Y - \frac{\alpha'}{2\pi a\sigma}c'_E\vec{\nabla}\times\vec{B}_Y. \tag{23}$$

Since $\vec{\nabla}\cdot\vec{B}_Y = 0$, we can write the hypermagnetic field as $\vec{B}_Y = (1/a)\nabla\times\vec{A}_Y$, where $\vec{A}_Y$ is the vector potential. Considering a fully helical hypermagnetic field, the following nontrivial Chern-Simons wave configuration for $\vec{A}_Y$ can be chosen [7,9,12,13,16,17,73–75]:

$$\vec{A}_Y = \gamma(t)(\sin kz, \cos kz, 0), \tag{24}$$

where $\gamma(t)$ is the time-dependent amplitude of $\vec{A}_Y$, and k is the comoving wave number. This topological configuration, which is an exact single-mode solution to the chiral magnetohydrodynamic equations [76,77], has been used extensively in the literature [7,9,16,17,72–75,78,79].

Choosing a helical configuration is desirable, since the coherent magnetic fields in the intergalactic medium have been inferred to be helical [80]. In fact, helical configurations are further motivated because they can theoretically be generated from inflationary models [79]. Having said that, even if one starts with a partially helical configuration, it would finally become maximally helical through an inverse cascade mechanism [76,81–83].

Using the configuration in Eq. (24), the hypermagnetic field becomes $\vec{B}_Y = (1/a)k\vec{A}_Y$, and consequently[12]

$$\vec{E}_Y = \frac{k'}{\sigma}\vec{B}_Y + \frac{\alpha'}{2\pi\sigma}c'_E\vec{B}_Y, \tag{25}$$

and

$$\partial_t\vec{B}_Y + 2H\vec{B}_Y = -\frac{k'^2}{\sigma}\vec{B}_Y - \frac{\alpha'}{2\pi\sigma}c'_Ek'\vec{B}_Y, \tag{26}$$

with $k' \equiv k/a = kT$, can be derived. Let us define the amplitude of the hypermagnetic field $(\vec{B}_Y)$ as $B_Y(t) \equiv k'\gamma(t)$. Hence, Eq. (26) can be rewritten as the following

$$\partial_t B_Y + 2HB_Y = -\frac{k'}{\sigma}B_Y\left(k' + \frac{\alpha'}{2\pi}c'_E\right). \tag{27}$$

Thus far, we have seen that if $\mu_i \neq 0$ (there is a nonzero asymmetry), $E_Y(t)$ and $B_Y(t)$ get modified due to the Chern-Simons term. The evolution of asymmetries, on the other hand, depends on $E_Y \cdot B_Y$. Therefore, the modified electric field and hypermagnetic field become important in the evolution of asymmetries. In the following section, we

[12]One might be concerned that choosing this configuration may violate our assumption of the homogeneity and isotropy condition. However, we show that in this setup, the maximum magnetic pressure $(B_Y^2/8\pi)$ is orders of magnitude smaller than the fluid pressure and thus the homogeneity and isotropy conditions as considered in the FRW metric remain valid [84,85].

will discuss how this effect shows up in the evolution of asymmetries in greater detail.

IV. EVOLUTION OF MATTER ASYMMETRIES

As mentioned earlier, with the simplifying assumptions that we have made, all matter asymmetries can be obtained in terms of the asymmetry of the right-handed electron. Therefore, it suffices to study the dynamics of this asymmetry, only [9]. The asymmetry in the number density of the right-handed electrons can be found by solving the following Boltzman equation:

$$\dot{n}_{e_R} + 3Hn_{e_R} = -\Gamma_{LR}\left(n_{e_R} - n_{e_L} + \frac{n_\phi}{2}\right) + B_e\Gamma_S n_S + \frac{\alpha'}{\pi}\vec{E}_Y\cdot\vec{B}_Y. \tag{28}$$

In the above equation, n_i with $i = \{e_R, e_L, \phi, S\}$, is the *difference* between the number densities of a particle and its antiparticle. The term involving H is due to the expansion of the Universe, and the term containing Γ_{LR} shows the effect of the electron Yukawa interaction. Note that the factor of $1/2$ in the parentheses is due to the spin statistics of the Higgs. Furthermore, the term $B_e\Gamma_S n_S$ comes from the decay of the flavon, with B_e being the flavon branching ratio to electrons:

$$B_e = \frac{g_e^2}{\sum_f g_f^2}, \qquad f = e, u, d. \tag{29}$$

Instead of n_S, it is more convenient to work with ρ_S. Therefore, we define a dimensionless parameter ξ_S as $\xi_S \equiv n_S m_S/\rho_S$, which does not depend on time. It should be noted that ξ_S is different from the canonical definition of $\eta_S \equiv n_S/s$, where s is the entropy density.

One important difference between our work and Ref. [39] is due to the term containing $\vec{E}_Y\cdot\vec{B}_Y$ in Eq. (28). This term comes from the Abelian anomaly equation:

$$\partial_\mu J^\mu_{e_R} = -\frac{1}{4}Y_R^2\frac{\alpha'}{4\pi}Y_{\mu\nu}Y^{\mu\nu} = \frac{\alpha'}{\pi}\vec{E}_Y\cdot\vec{B}_Y, \tag{30}$$

where $Y_R = -2$ is the hypercharge of the right-handed electron. The above equation relates the evolution of number densities to that of the helicity of the hypermagnetic field. Using Eq. (25), we can derive

$$\vec{E}_Y\cdot\vec{B}_Y = \frac{B_Y^2}{\sigma}\left(k' + \frac{\alpha'}{2\pi}c'_E\right). \tag{31}$$

As can be seen, the CME is not only important for the evolution of the hypermagnetic field as discussed in the previous section, but also it has a non-trivial effect on the evolution of the asymmetries via the term containing c'_E. Previously, we had defined c'_E in terms of the chemical potential of right-handed electron: $c'_E = -99/37\mu_{e_R}$. We can convert μ_{e_R} to n_{e_R} using $n_{e_R} = \mu_{e_R}T^2/6$.

In the subsequent section, we solve the coupled differential equations for ρ_S, $\rho_{\rm rad}$ [Eq. (9)], B_Y [Eq. (27)], and n_{e_R} [Eq. (28)] numerically. To fully comprehend different stages of the evolutions, we first discuss one specific benchmark. We then move on to scanning the parameter space to find the desired region of the parameter space.

V. NUMERICAL STUDY

In this section, we do a numerical study of the coupled evolution equations of ρ_S, $\rho_{\rm rad}$, B_Y, and n_{e_R} from $T_\star$ up to $T_{\rm EW}$. Our free parameters are $T_\star, m_S, \Lambda, \xi_S, k, B_Y(T_\star)$. Before diving into the numerical analysis, let us make a few comments on these parameters:

(i) We need the flavon production to stay out of equilibrium during coherent oscillation. Hence, the maximum value of $T_\star$ should be $T_{\rm max}(\Lambda)$, as defined earlier.

(ii) By looking at the evolution equations, we see that the ratio of m_S/Λ is a recurring variable. Thereby, we find it more convenient to work with $\epsilon_m \equiv m_S/\Lambda$, and Λ instead of m_S and Λ. In order to respect EFT, we require $\epsilon_m \ll 1$.

(iii) It has been shown that for $k \gtrsim 10^{-7}$, the hypermagnetic field does not survive the Ohmic dissipation in the plasma [7]. In our numerical analysis, we rescale k and work with $c_{k_0} \equiv k/10^{-7}$, instead.

(iv) As can be seen in Eq. (27), a nonzero initial seed is needed for the hypermagnetic field to be later amplified as a result of the CME.[13] Here, we fix the initial amplitude of the hypermagnetic field to a small value of $B_Y(T_\star) = 0.01$ G.

(v) In our scenario, we need large matter asymmetries in order to obtain the desired value of $B_Y(T_{\rm EW}) \gtrsim 10^{19}$ G, as explained earlier. Since the flavon is responsible for the generation of these asymmetries, we fix ξ_S to its maximum value: $\xi_S = 1$.

(vi) We further assume that all initial asymmetries in the fermionic sector are zero (i.e., $\eta_f(T_\star) = 0$).

According to the above assumptions, the free parameters we work with in this paper, are

$$T_\star, \qquad \epsilon_m, \qquad \Lambda, \qquad c_{k_0}.$$

A. A case study

In this subsection, we present a careful study of the evolution of $\eta_B(T)$ and $B_Y(T)$ as a function of temperature for the following benchmark:

[13]The creation of the seed is beyond the scope of this study. Interested readers are encouraged to look into Refs. [72,86–94] on some of the possible mechanisms for the production of this seed.

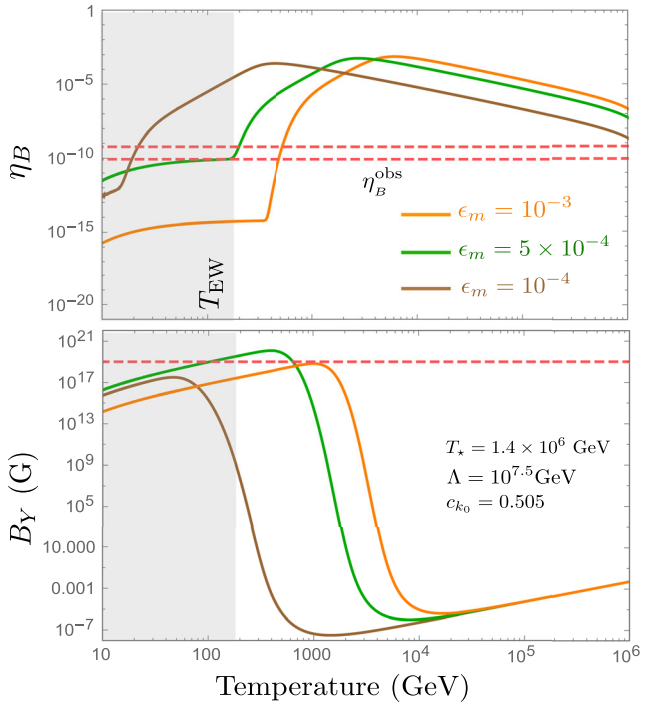

FIG. 2. The evolutions of η_B (upper panel) and B_Y (lower panel) as a function of temperature for $\epsilon_m = 10^{-3}$ (Orange), $\epsilon_m = 5\times10^{-4}$ (Green), and $\epsilon_m = 10^{-4}$ (Brown) are presented. These plots are for the fixed values of $\Lambda = 10^{7.5}$ GeV, $T_\star = 1.4\times10^6$ GeV, and $c_{k_0} = 0.505$. As a result of the flavon decay at high temperatures, the asymmetries grow. Once η_B reaches a large enough value, the hypermagnetic fields start getting amplified at the expense of eating some of the asymmetries. This process continues until the expansion rate of the universe becomes more important than the CME.

$$\Lambda = 10^{7.5}\ \text{GeV}, \qquad \epsilon_m = 5\times10^{-4},$$
$$T_\star \simeq 1.4\times10^6\ \text{GeV}, \qquad c_{k_0} = 0.505, \tag{32}$$

where $T_\star$ is chosen as $T_{\rm max}(\Lambda)$ for $\Lambda = 10^{7.5}$ GeV. The above parameters are chosen such that the desired values of $\eta_B(T_{\rm EW}) \simeq 10^{-10}$ and $B_Y(T_{\rm EW}) \gtrsim 10^{19}$ G are obtained. To see how other benchmarks may change the results, we present the plots of $\eta_B(T)$ and $B_Y(T)$ for three different values of $\epsilon_m = 10^{-3}, 5\times10^{-4}, 10^{-4}$ in Fig. 2; the values of $\Lambda, T_\star$, and c_{k_0} are fixed as Eq. (32).[14]

As mentioned earlier, the evolution of η_B is intimately related to that of η_{e_R}: $\eta_B = \frac{198}{481}\eta_{e_R}$. Therefore, by solving Eq. (28), we are practically obtaining the evolution of η_B. To discuss the physical effects important in each time interval of the evolution, the evolution of the terms contributing to $\dot\eta_{e_R}/\eta_{e_R}$ [Eq. (33)] and $\dot B_Y/B_Y$ [Eq. (27)] are shown in Figs. 3 and 4.

[14]It is worth mentioning that η_B and B_Y are highly sensitive to the exact value of c_{k_0}, and thus its value should be carefully tuned, as will be shown in the next subsection.

To accomplish this task, let us first rewrite Eq. (27) as

$$\frac{\dot B_Y}{B_Y} = -2H - \frac{k'}{B_Y^2}(\vec E_Y\cdot\vec B_Y),$$

where $\vec E_Y\cdot\vec B_Y$ in Eq. (31) can also be separated as

$$(\vec E_Y\cdot\vec B_Y)_{\text{non-CME}} \equiv \frac{B_Y^2}{\sigma}k',$$
$$(\vec E_Y\cdot\vec B_Y)_{\text{CME}} \equiv \frac{B_Y^2}{\sigma}\cdot\frac{\alpha'}{2\pi}c_E'.$$

Note that, here, c_E' is a negative quantity, therefore the effect of $(\vec E_Y\cdot\vec B_Y)_{\text{CME}}$ and $(\vec E_Y\cdot\vec B_Y)_{\text{non-CME}}$ are opposite of each other.

Similarly, let us rewrite Eq. (28) in terms of η_{e_R}:

$$\dot\eta_{e_R} + \frac{3}{4}\frac{\rho_S}{\rho_{\rm rad}}\Gamma_S\eta_{e_R} = -\Gamma_{LR}\left(\eta_{e_R} - \eta_{e_L} + \frac{\eta_\phi}{2}\right) + B_e\Gamma_S\frac{n_S}{s} + \frac{\alpha'}{\pi s}\vec E_Y\cdot\vec B_Y, \tag{33}$$

where the derivation of this equation is presented in Appendix A. Notice that the second term comes from the domination of the flavon after $T_\star$.

According to Figs. 3 and 4, the following critical temperatures can be distinguished:

(i) $T_{B_Y(\rm min)}$: This is the temperature at which the HMFA is at its minimum.
(ii) $T_{B_Y(\rm max)}$: This is when the HMFA reaches its maximum.
(iii) $T_s^{\rm max}$: this is when the deviation of the Hubble rate from the SC Hubble rate is maximum.
(iv) $T_{\rm cf}$: As explained earlier (Fig. 1), this is the temperature at which the chirality flip rate of the electrons equals the Hubble rate.
(v) $T_{E\cdot B}^{\text{non-CME}}$: This is the temperature at which the baryonic asymmetry saturates and becomes flat. As can be seen from Fig. 4, this is the temperature at which the non-CME component of Eq. (28) becomes the dominant effect that leads to an increase in the asymmetry.

1. The evolution of $B_Y(T)$

Now that we have identified the critical temperatures, we can move on to discussing the following intervals of temperature, which are identified in Fig. 3:

(i) $T_{B_Y(\rm min)} < T < T_\star$: In this interval, the Hubble rate is higher than $\frac{k'}{B_Y^2}(E_Y\cdot B_Y) \simeq \frac{k'}{B_Y^2}(E_Y\cdot B_Y)_{\rm CME}$, as illustrated in the $\dot B_Y/B_Y$ plot. This leads to a decrease of $B_Y(T)$ according to the expansion of the Universe.

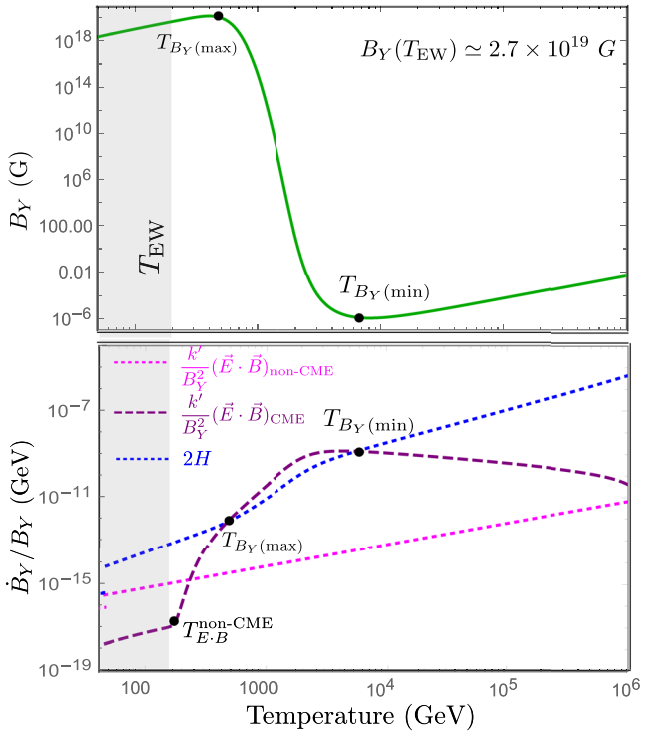

FIG. 3. The evolution of B_Y as a function of temperature is illustrated in the upper panel, while the lower panel shows the terms contributing to $\dot{B}_Y/B_Y$. The CME component (shown by dashed purple) leads to an increase in the HMFA, and the non-CME component (dotted magenta) reduces B_Y. We see that once the $(\vec{E}_Y \cdot \vec{B}_Y)$ contribution exceeds the Hubble rate (dotted blue), the hypermagnetic field starts increasing and this trend continues until it falls below the Hubble rate again.

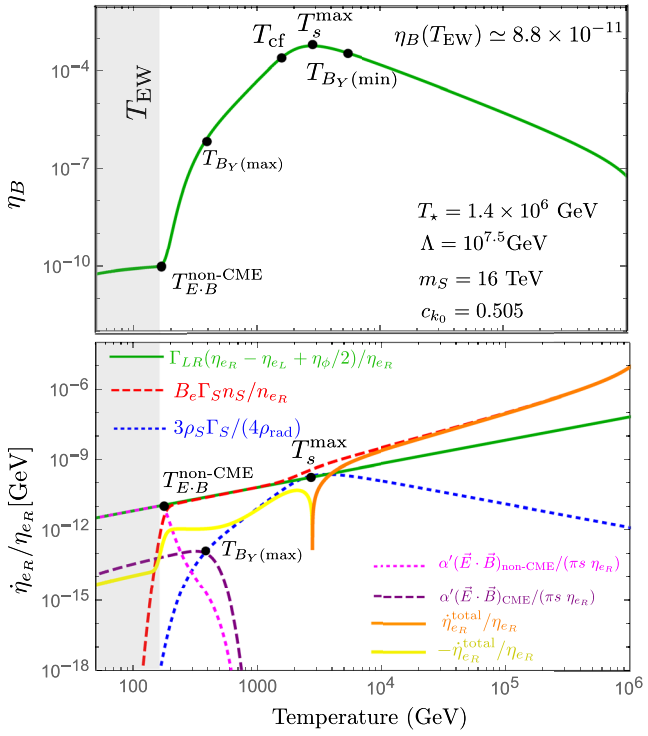

FIG. 4. The evolution of η_B for the benchmark (32) as a function of temperature is presented in the upper panel. The lower panel is each of the contributions to $\dot{\eta}_{e_R}$ [Eq. (33)] normalized by η_{e_R}, the quantity which is equal to $\dot{\eta}_B/\eta_B$ as well. In the lower panel, the solid green line is proportional to the rate of the chirality flip of the right-handed electron. The dashed red line is the relative growth rate of the asymmetry in the right-handed electron injected by the flavon. The dotted blue line is the contribution of the flavon to the dilution of the asymmetry. The dotted magenta and the dashed purple line, respectively, show the non-CME and the CME components of the hypermagnetic field effect in the evolution of η_B. The solid orange and yellow lines, together, show the magnitude of the sum of the contributions. Among the contributions, the flavon decay and the non-CME component of $(\vec{E}_Y \cdot \vec{B}_Y)$ increase the asymmetry while the rest results in a lower asymmetry. In this benchmark, the gap between when the flavon decays exponentially and when $(\vec{E}_Y \cdot \vec{B}_Y)_{\rm non\text{-}CME}$ dominates is small and that is one of the main reasons that the asymmetry is saved at good values.

(ii) $T_{B_Y(\max)} < T < T_{B_Y(\min)}$: Here, the HMFA increases rapidly due to the domination of the $\frac{k'}{B_Y^2}(E_Y \cdot B_Y)_{\rm CME}$ over the Hubble rate. As emphasized earlier, this is the term that makes the growth of the HMFA possible.

(iii) $T_{\rm EW} < T < T_{B_Y(\max)}$: In this interval, the Hubble rate dominates, which once again leads to the decrease of the HMFA according to the expansion of the Universe.

2. The evolution of $\eta_B(T)$

Similarly, to better comprehend the evolution of the asymmetries, let us study the plots shown in Fig. 4. The upper panel is η_B and the lower panel is the magnitude of each of the contributions to $\frac{\dot{\eta}_B}{\eta_B} = \frac{\dot{\eta}_{e_R}}{\eta_{e_R}}$, as a function of temperature.

In the lower panel, the solid green line is proportional to the rate of the chirality flip of the right-handed electron, which leads to the wash out of the asymmetry by the weak sphalerons. Notice that due to our choice of *y-axis*, this term is independent of η_B. The dashed red line is the relative growth rate of the asymmetry in the right-handed electron coming from the flavon. If η_{e_R} is leaning toward zero, this term becomes greater and prevents the asymmetry from depleting. The dotted blue line represents the term that appears due to the domination of ρ_S (and the decay of the flavon to radiation) at high temperatures.[15] This term is also independent of η_B and, we will refer to it as the dilution term.

[15]It is worth mentioning that in the SC, this term does not appear.

As discussed earlier, the term coming from the Abelian anomaly has two contributions: $(\vec{E}_Y \cdot \vec{B}_Y)_{\rm CME}$ (the dashed purple line) which eats up part of the asymmetry to amplify the HMFA, and $(\vec{E}_Y \cdot \vec{B}_Y)_{\text{non-CME}}$ (the dotted magenta line) which leads to an increase in the asymmetry. The CME component is independent of η_B, but the non-CME component is proportional to the inverse of η_B. Hence, we see that the terms leading to an increase in the asymmetry are sensitive to η_B and they grow if $\eta_B \to 0$. This is a reassurance that the system wants to save the asymmetry as much as possible.[16] Finally, the solid orange and the yellow line represents the sum and the negative sum of all of these contributions. In the following, we discuss the main players in each of the temperature intervals.

(i) $T_s^{\rm max} \lesssim T < T_\star$: Here, the evolution of η_B is mostly governed by the flavon, the effect of which is twofold: the production of asymmetry due to the decay of the flavon, and the dilution of the asymmetry due to its effect on the expansion of the Universe (dashed blue line). As we reach $T_{\rm cf}$, the chirality flip of the electron becomes relevant as well, slowing down the increase in the asymmetry. Notice that at $T_s^{\rm max}$, there is a cancellation between the terms that increase the asymmetry and those that lead to the reduction of the asymmetry. This feature is consistent among all of the benchmarks that yield the desired values of η_B and B_Y [Eq. (14)]. Thus, the asymmetry is increasing up until $T_s^{\rm max}$, and after that starts decaying. Comparing Figs. 3 and 4, we see that once the asymmetry becomes greater than $\eta_B \gtrsim 2 \times 10^{-4}$, the HMFA starts increasing, and thus $T_{B_Y(\rm max)} < T_s^{\rm max} < T_{B_Y(\rm min)}$.

(ii) $T_{E\cdot B}^{\text{non-CME}} \lesssim T \lesssim T_s^{\rm max}$: During this interval, the rate of chirality flip of the right-handed electron (or equivalently, the rate of the washout of the asymmetry due to the sphalerons) exceeds[17] the production rate of asymmetry through the flavon decay. As a result, the asymmetry decreases. Nonetheless, as can be seen from Fig. 4, these two rates are almost compatible, preventing the asymmetry from diminishing too quickly. This is an example of how the *gradual* decay of the flavon to right-handed electron helps to retain the asymmetry in the fermions.

(iii) $T_{\rm EW} < T < T_{E\cdot B}^{\text{non-CME}}$: As we reach $T_{E\cdot B}^{\text{non-CME}}$, the non-CME component of $\vec{E}_Y \cdot \vec{B}_Y$ becomes compatible with the rate of electron chirality flip, which slows down the decrease of the asymmetry significantly. In other words, the amplified hypermagnetic field feeds back to the asymmetry and helps to preserve the asymmetry. Therefore, during this interval, the asymmetry is almost constant. In general, a successful benchmark is the one that there is not a large gap between $T_{E\cdot B}^{\text{non-CME}}$ and the temperature at which the flavon decays exponentially. If this gap is large, the sphalerons have enough time to wash out the asymmetry quickly.

Now that we have discussed each of the important intervals, let us scan through the parameter space and indicate the sweet regions that give the desired values at $T_{\rm EW}$ [Eq. (14)]. Before that, however, allow us to emphasize two features of this benchmark that made it desirable: (1) For (most of) the temperatures below $T_s^{\rm max}$, the terms leading to an increase in the asymmetry are compatible with the ones that cause the asymmetry to decrease. Generally, this means that either the flavon is long-lived which then injects the asymmetry to the fermionic sector gradually and pushes $T_{\rm cf}$ closer to $T_{\rm EW}$ as well, and/or the gap between $T_{E\cdot B}^{\text{non-CME}}$ and the temperature at which the flavon decays exponentially is very small. (2) There is enough time for the hypermagnetic field to grow before $T_{\rm EW}$ (e.g., $T_{B_Y(\rm max)} > T_{\rm EW}$). However, if $T_{B_Y(\rm max)}$ is at very high temperatures (e.g., $T_{B_Y(\rm max)} \sim T_s^{\rm max}$), the $(\vec{E}_Y \cdot \vec{B}_Y)$ terms govern the evolution of η_B and the sphalerons become subdominant. Therefore, the asymmetry is restored at higher values than desired. Some of the examples of this case will be indicated in the next subsection. In the following, we show the $\eta_B(T_{\rm EW})$ and $B_Y(T_{\rm EW})$ as a function of various parameters.

B. Scanning parameter space

In this section, we scan through the parameter space and find $\eta_B(T_{\rm EW})$ and $B_Y(T_{\rm EW})$ for various values of $\Lambda, \epsilon_m, T_\star$ and c_{k_0}. From a few test runs, we realize that Λ should live in a narrow range of 5×10^6 GeV $\lesssim \Lambda \lesssim 5 \times 10^9$ GeV. For $\Lambda < 5 \times 10^6$ GeV, the maximum temperature ($T_{\rm max}$) must be below 10^4 GeV, which means that the chirality flip of the right-handed electron process is in equilibrium from the beginning of the Universe, and therefore the weak sphalerons will wash out the asymmetry in the SM fermions as soon as the flavon starts decaying. Thereby, for $\Lambda < 5 \times 10^6$ GeV, we get $\eta_B(T_{\rm EW}) \ll \eta_B^{\rm obs}$ and the hypermagnetic field does not have a chance to amplify. For $\Lambda \gtrsim 10^9$ GeV, the decay width is too large such that flavon decays too quickly. Thus, the flavon cannot help with the preservation of the asymmetry in the early universe. In other words, $T_{\rm cf} \gg T_{\rm EW}$ and the weak sphalerons wash out the asymmetry.

Figure 5 presents the baryon asymmetry of the Universe and the HMFA at $T = T_{\rm EW}$ as a function of ϵ_m. Different curves represent different values of Λ, and we have fixed $T_\star = T_{\rm max}(\Lambda)$ and $c_{k_0} = 0.505$. For a fixed Λ, if ϵ_m is very small ($\ll 10^{3.5}$ GeV$/\Lambda$ or equivalently

[16] It is clear that the physics would not change if we had plotted $\dot{\eta}_B$ instead of $\dot{\eta}_B/\eta_B$.

[17] To be more exact, the dilution term (dotted blue line) is also important in decreasing the asymmetry. This is especially true for temperatures closer to $T_s^{\rm max}$. However, this term quickly drops and its effect becomes negligible at lower temperatures.

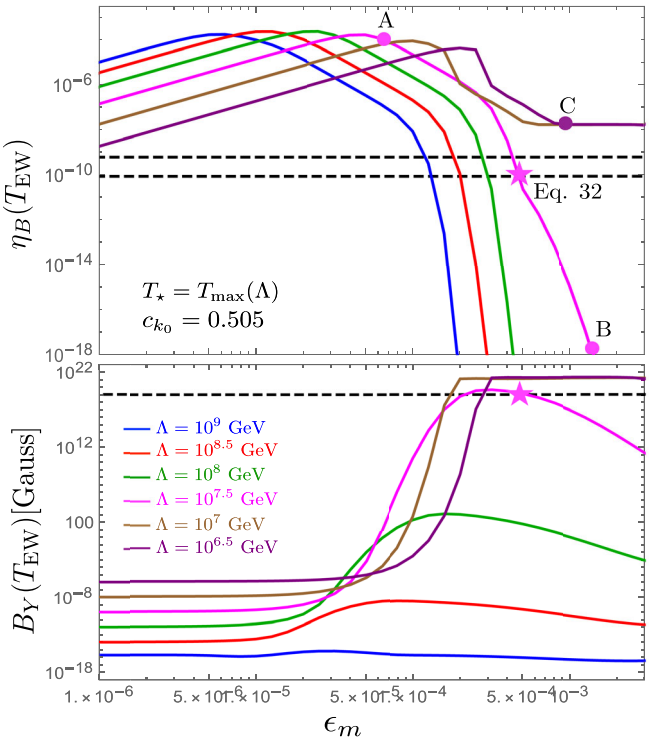

FIG. 5. The dependence of η_B (upper panel) and hypermagnetic field amplitude B_Y (lower panel) on the mass of the flavon m_S. The solid lines represent different cut-off scales Λ.

$m_S \ll 3$ TeV-Benchmark A), the injection of asymmetry from the flavon to right-handed electron occurs at a slow rate. This effect has two consequences; (1) we move away from SC so much that $T_{\rm cf}$ is after $T_{\rm EW}$, and (2) the asymmetry is not large enough to amplify the HMFA. Since $T_{\rm cf} < T_{\rm EW}$, the value of $\eta_B(T_{\rm EW})$ will just depend on the work of the flavon. Therefore, in this regime, as we increase ϵ_m we see that $\eta_B(T_{\rm EW})$ is increasing because more of the flavon has decayed into the right-handed electron. An example of such a case is studied in Appendix B.

On the other extreme, for large ϵ_m, the flavon decays too quickly.[18] In this scenario, the value of $\eta_B(T_{\rm EW})$ is intimately connected to the HMFA. If B_Y has not been amplified, the effect of $(\vec{E}_Y \cdot \vec{B}_Y)$ is negligible and the sphalerons have enough time to eat up the asymmetry. Hence, in such cases, we see that both $\eta_B(T_{\rm EW})$ and $B_Y(T_{\rm EW})$ are small (e.g., Benchmark B). If B_Y has been amplified, the battle between $(\vec{E}_Y \cdot \vec{B}_Y)_{\text{non-CME}}$ + flavon decay vs $(\vec{E}_Y \cdot \vec{B}_Y)_{\rm CME}$ determines the evolution of η_B and the effect of the chirality flip of right-handed electrons is negligible (e.g., Benchmark C). Let us mention that benchmark C will be acceptable if we relax the assumption that the value of η_B and B_Y stay fixed during and after the EWPT.

For some values of Λ, the intermediate values of ϵ_m yield Eq. (14). That comes from a delicate work of nonstandard cosmology (domination of ρ_S), and the effect of $(\vec{E}_Y \cdot \vec{B}_Y)_{\text{non-CME}}$ at lower temperatures. Both of these effects are important in taming the work of sphalerons, as explained in Sec. V A.

Another free parameter that can affect the baryon asymmetry and especially hypermagnetic field is c_{k_0}. As the plots in Fig. 6 show, the results are sensitive to c_{k_0} and we cannot choose an arbitrary small c_{k_0} value. Since $c_{k_0} \leq 1$, it mainly affects the HMFA through the CME contribution to its evolution equation. Interestingly, the value of c_{k_0} is particularly important in the non-CME

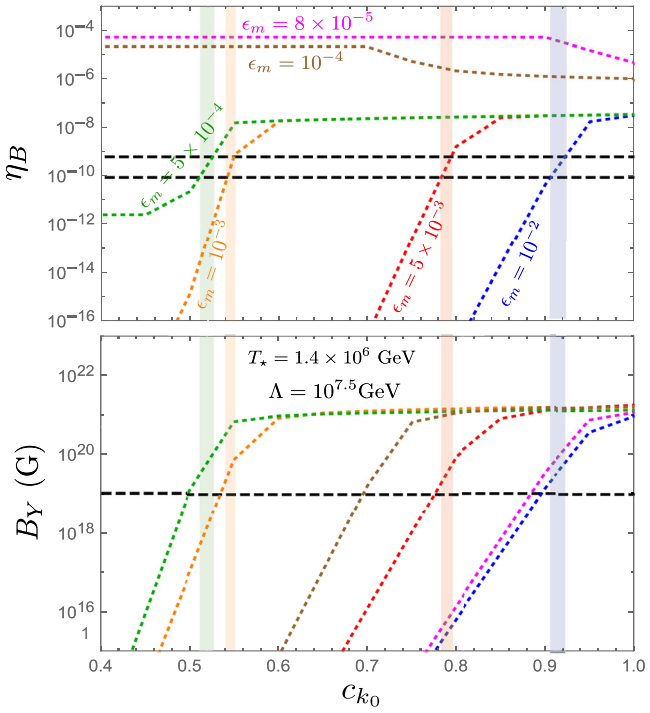

FIG. 6. The dependence of η_B (upper panel) and hypermagnetic field amplitude B_Y (lower panel) on c_{k_0}. Each of the dashed lines represent a fixed ϵ_m, and for all of the curves, we have fixed $\Lambda = 10^{7.5}$ GeV. The results are highly sensitive to the value of c_{k_0} and in general the closer we get to $c_{k_0} = 1$, the higher the values of η_B and B_Y become. Near $c_{k_0} = 1$, we see a stabilization for all of the values of ϵ_m we considered. For $\epsilon_m \lesssim 10^{-4}$ we see that we consistently get a large value of η_B, while B_Y exponentially decreases to zero.

[18]Note that Γ_S is proportional to $\epsilon_m^3 \Lambda$, and thus as we increase either of ϵ_m or Λ, the decay width of the flavon increases and the flavon decays faster. However, the injection of asymmetry to the right-handed electron is proportional to $\Gamma_S/m_S = \epsilon_m$, and an increase in ϵ_m causes more asymmetry to be transferred to the right-handed electron. Thereby, for large ϵ_m, depending on the value of Λ, we either end up with too much asymmetry (Benchmark C) or too little asymmetry (Benchmark B).

contribution to the evolution of the asymmetry, whose main role is to save the asymmetry at temperatures closer to $T_{\rm EW}$. Therefore, as illustrated in Fig. 6, large values of c_{k_0} will result in large $\eta_B(T_{\rm EW})$ and $B_Y(T_{\rm EW})$. Similarly, for small values of c_{k_0}, the opposite is true. However, if ϵ_m is very small, the evolution of η_B is only determined by the flavon dynamics (see Appendix B) and it is independent of $(\vec{E}_Y \cdot \vec{B}_Y)$. In these cases (e.g., $\epsilon_m = 8 \times 10^{-5}, 10^{-4}$ in Fig. 6), the baryonic asymmetry at $T = T_{\rm EW}$ will remain large even for small c_{k_0}. The desirable values of c_{k_0} for each ϵ_m is presented by a shaded band in Fig. 6.

Yet, one other parameter that can leave an impact on the final result is the value of $T_\star$. We have discussed the maximum value of $T_\star$, but technically we can choose any $T_\star$ less than $T_{\rm max}$. By examining different values of $T_\star$, we noticed that only $T_\star = T_{\rm max}$ gives the best results. If $T_\star \ll T_{\rm max}$, the flavon does not have enough time to efficiently transfer its asymmetry to the fermionic sector and eventually leads to the amplification of the HMFA.

VI. CONCLUSION

In this paper, we discussed the possibility of the simultaneous generation of baryonic asymmetry to $\eta_B(T_{\rm EW}) \sim 8.5 \times 10^{-11}$ and the amplification of HMFA from a small seed to $B_Y(T_{\rm EW}) \sim 10^{20}$ G in the presence of a flavon that carries a large asymmetry ($\xi_S = 1$). We found a successful scenario that lives in a region where the cutoff scale is $\sim 10^{7.5}$ GeV. Given the cutoff scale, the mass of the flavon could vary over a small range of values to give a desirable outcome. Another free parameter that played an important role in the dynamics of baryonic asymmetry and HMFA was the comoving wave number of the hypermagnetic field. According to our study, the comoving wave number should be $(0.5 - 1) \times 10^{-7}$. In general, we found there is a strong sensitivity to each of these parameters. A small change could result in a drastic change in the results. This is because we need a delicate cancellation between the terms that increase the asymmetry and the ones that result in a lower asymmetry, and thus we have to choose our parameters carefully.

For most of the parameter space, we get a large asymmetry of the Universe, while having a small (compared to the desired) value of HMFA. This occurs because the asymmetry in the flavon transfers into baryonic asymmetry, but there is not enough time for the HMFA to grow. This occurs in the benchmarks where the flavon is very long-lived and it transfers its asymmetry to the fermionic sector at a very small pace. The baryonic asymmetry must reach above $\eta_B > 2 \times 10^{-4}$ for the HMFA to start growing. When the flavon decays too slowly, the baryonic asymmetry reaches 2×10^{-4} either very close or even after the electroweak temperature. Therefore, the HMFA remains small.

On the other hand, if the flavon is very short-lived, we may have two very different cases depending on the value of Λ: (1) For sufficiently small Λ, the flavon injects its asymmetry to fermionic sector quickly and causes the HMFA to grow fast. The hypermagnetic field then feeds back to the asymmetry and prevents it from being washed out. In such scenarios, we noticed that we end up with a larger η_B than expected. (2) for a relatively bigger Λ, we may also have a case where the injection of asymmetry is inefficient and we end up with a very small η_B.

The value of the comoving wave number has an indisputable effect on the HMFA and thus has a great influence on the baryonic asymmetry as well. We noticed that to get the observed value of η_B and the desired value of $B_Y(T_{\rm EW})$, we have to live in a small region of the parameter space and thus our scenario is predictive.

In this paper, we considered a configuration of $\vec{B}_Y$ that would naively violate the homogeneity and isotropy condition of the FRW metric. However, the maximum hypermagnetic field amplitude in our study is about 10^{21} G, which means that the ratio of the magnetic pressure to the fluid pressure is less than 10^{-6}. Hence, we are safe that with this configuration, the homogeneity and isotropy conditions remain valid to a good approximation. Moreover, we only considered the coupling of the flavon with the first generation of fermions. This choice was suitable because the branching ratio of the flavon to electrons was enhanced. In fact, we could not find a benchmark that could explain both baryogenesis and magnetogenesis with other choices of flavon coupling. Having said that, the assumption of flavon coupling to only the first generation of fermions is theoretically justifiable as well. That is because the first generation of fermions is much lighter than the electroweak scale. Thus, explaining their small Yukawa couplings is of priority.

ACKNOWLEDGMENTS

We would like to thank S. Ipek, J. Kopp, H. Mehrabpour, M. Shaposhnikov, and G. White for numerous useful conversations. We are also thankful to the CERN theory division and Mainz Cluster of Excellence for their hospitality. We also would like to express our gratitude to B. Enshaeian for his continuous support.

APPENDIX A: EVOLUTION OF η_R

The asymmetry in the number density of the right-handed electrons is governed by the following Boltzman equation:

$$\dot{n}_{e_R} + 3Hn_{e_R} = -\Gamma_{LR}\left(n_{e_R} - n_{e_L} + \frac{n_\phi}{2}\right) + B_e\Gamma_S n_S + \frac{\alpha'}{\pi}\vec{E}_Y \cdot \vec{B}_Y. \quad \text{(A1)}$$

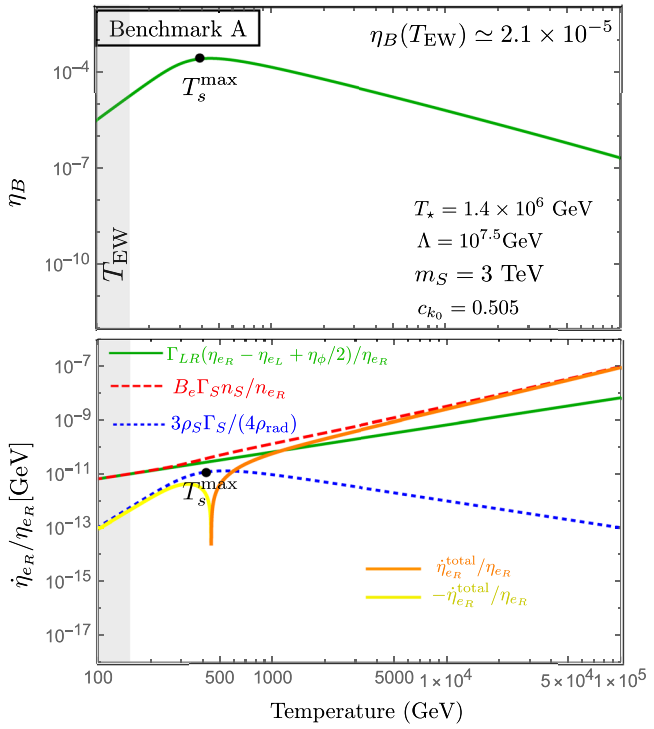

FIG. 7. The evolution of η_B for benchmark A as a function of temperature is presented. The lower panel is each of the contributions to $\dot\eta_{e_R}$ [Eq. (33)] normalized by η_{e_R}, the quantity which is also equal to $\frac{\dot\eta_B}{\eta_B}$. In the lower panel, the solid green line is proportional to the rate of the chirality flip of the right-handed electron. The dashed red line is the relative growth rate of the asymmetry in the right-handed electron injected by the flavon. The dotted blue line is the contribution of the flavon to the dilution of the asymmetry. The solid orange and yellow lines, together, show the magnitude of the sum of the contributions. In this benchmark, the asymmetry is slowly transferring from the flavon to the right-handed electron. This rate is very small, which means the rate of flavon depletion is small. Hence the cosmology becomes very nonstandard. In this case, $T_{\rm cf}$ occurs too close to $T_{\rm EW}$, and thus the asymmetry is not washed out efficiently. Hence, we end up with too large $\eta_B(T_{\rm EW})$. The HMFA does not have a chance to grow and stays close to its initial value.

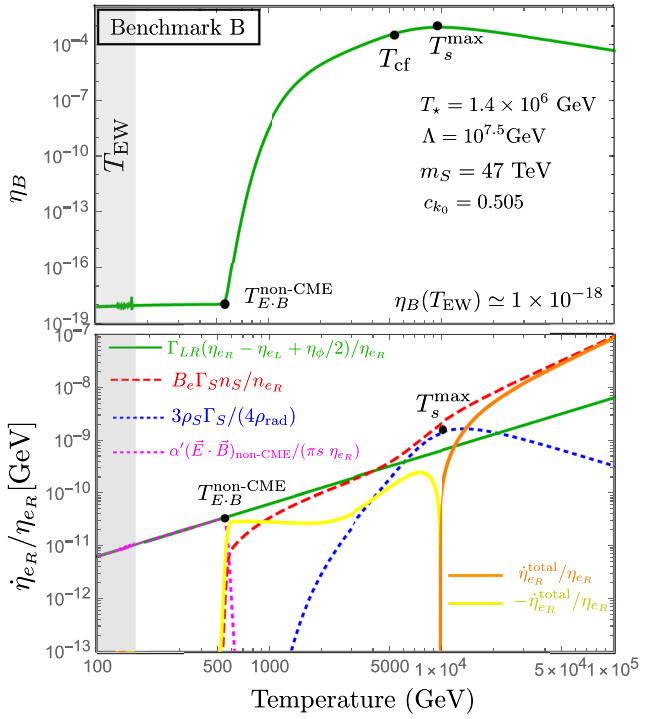

FIG. 8. The evolution of η_B for benchmark B as a function of temperature is presented. The lower panel is each of the contributions to $\dot\eta_{e_R}$ [Eq. (33)] normalized by η_{e_R}, the quantity which is also equal to $\frac{\dot\eta_B}{\eta_B}$. In the lower panel, the solid green line is proportional to the rate of the chirality flip of the right-handed electron. The dashed red line is the relative growth rate of the asymmetry in the right-handed electron injected by the flavon. The dotted blue line is the contribution of the flavon to the dilution of the asymmetry. The dotted magenta shows the non-CME component of the hypermagnetic field effect in the evolution of η_B. The solid orange and yellow lines, together, show the magnitude of the sum of the contributions. In this benchmark, there is a large gap between when the flavon decays and $(\vec E_Y\cdot\vec B_Y)_{\rm non\text{-}CME}$ dominates. During this gap, the sphaleron has enough time to eat up the asymmetry and thus we are left with too little asymmetry. Since the asymmetry depletes very quickly, the CME cannot increase the HMFA efficiently.

By dividing both sides by the comoving entropy,[19] s, we can convert this equation to an equation describing the evolution of η_{e_R}.

$$\dot\eta_{e_R} + 3\eta_{e_R}\frac{\dot T}{T} + 3H\eta_{e_R} = -\Gamma_{LR}\left(\eta_{e_R} - \eta_{e_L} + \frac{\eta_\phi}{2}\right) + B_e\Gamma_S\frac{n_S}{s} + \frac{\alpha'}{\pi s}\vec E_Y\cdot\vec B_Y \qquad \text{(A2)}$$

On the other hand, by definition we know $\dot T/T = 1/4\dot\rho_{\rm rad}/\rho_{\rm rad}$. This is while we can use Eq. (9) to find $\dot\rho_{\rm rad}/\rho_{\rm rad}$:

[19]Note that

$$\dot\eta = \frac{d(n/s)}{dt} = \frac{\dot n}{s} - \frac{n}{s^2}\frac{ds}{dT}\dot T = \frac{\dot n}{s} - 3\frac{n}{s}\frac{\dot T}{T}.$$

$$\frac{\dot\rho_{\rm rad}}{\rho_{\rm rad}} + 4H = \Gamma_S\frac{\rho_S}{\rho_{\rm rad}}. \qquad \text{(A3)}$$

Hence, Eq. (A2) becomes

$$\dot\eta_{e_R} + \frac{3}{4}\frac{\rho_S}{\rho_{\rm rad}}\Gamma_S\eta_{e_R} = -\Gamma_{LR}\left(\eta_{e_R} - \eta_{e_L} + \frac{\eta_\phi}{2}\right) + B_e\Gamma_S\frac{n_S}{s} + \frac{\alpha'}{\pi s}\vec E_Y\cdot\vec B_Y \qquad \text{(A4)}$$

In the SC, $\rho_S \simeq 0$, and thus the second term is negligible. In our case, however, the second term becomes important in some interval of the temperature.

APPENDIX B: BAD BENCHMARKS

Here we show the η_B evolution for the benchmarks shown in Fig. 5.

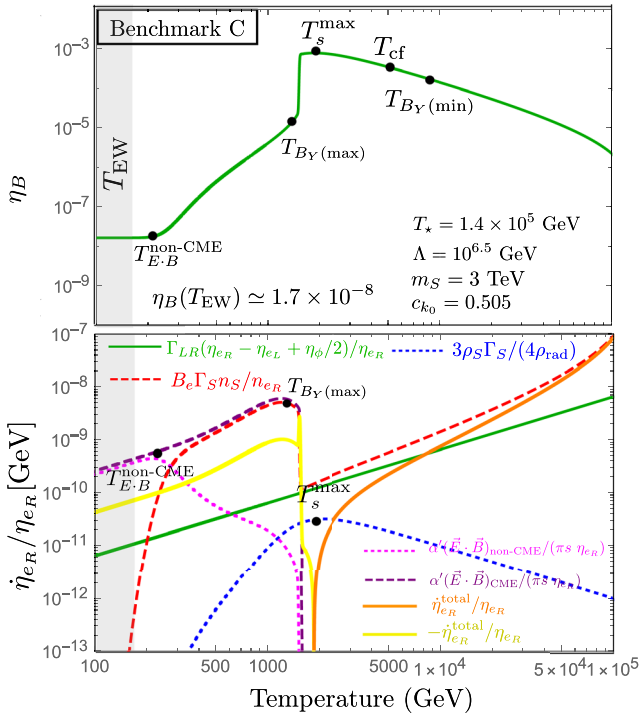

FIG. 9. The evolution of η_B for benchmark C as a function of temperature is presented. The lower panel is each of the contributions to $\dot\eta_{e_R}$ [Eq. (33)] normalized by η_{e_R}, the quantity which is also equal to $\frac{\dot\eta_B}{\eta_B}$. In the lower panel, the solid green line is proportional to the rate of the chirality flip of the right-handed electron. The dashed red line is the relative growth rate of the asymmetry in the right-handed electron injected by the flavon. The dotted blue line is the contribution of the flavon to the dilution of the asymmetry. The dotted magenta and the dashed purple line, respectively, show the non-CME and the CME components of the hypermagnetic field effect in the evolution of η_B. The solid orange and yellow lines, together, show the magnitude of the sum of the contributions. In this benchmark, the flavon decays quickly and thus increases the asymmetry in e_R at relatively high temperatures. Due to the increase in the asymmetry, the HMFA has enough time to amplify and even dominate the effect of the sphaleron. We see a sharp drop in the asymmetry at $T_{B_Y(\max)}$ followed by another decline. Both of these effects are due to the CME. Eventually, the non-CME component dominates and preserves the asymmetry. However, the value at which it preserves the asymmetry is larger than the observed value. Notice that the sharp increase in the flavon term is because of the normalization.

[1] R. Cooke, M. Pettini, R. A. Jorgenson, M. T. Murphy, and C. C. Steidel, Precision measures of the primordial abundance of deuterium, Astrophys. J. **781**, 31 (2014).

[2] P. A. R. Ade *et al.* (Planck Collaboration), Planck 2015 results. XIII. Cosmological parameters, Astron. Astrophys. **594**, A13 (2016).

[3] A. D. Sakharov, Violation of *CP* invariance, C asymmetry, and baryon asymmetry of the universe, Sov. Phys. Usp. **34**, 392 (1991).

[4] M. Fukugita and T. Yanagida, Barygenesis without grand unification, Phys. Lett. **174B**, 45 (1986).

[5] I. Affleck and M. Dine, A new mechanism for baryogenesis, Nucl. Phys. **B249**, 361 (1985).

[6] V. B. Semikoz and J. W. F. Valle, Chern-simons anomaly as polarization effect, J. Cosmol. Astropart. Phys. 11 (2011) 048.

[7] M. Dvornikov and V. B. Semikoz, Lepton asymmetry growth in the symmetric phase of an electroweak plasma with hypermagnetic fields versus its washing out by sphalerons, Phys. Rev. D **87**, 025023 (2013).

[8] V. A. Kuzmin, V. A. Rubakov, and M. E. Shaposhnikov, On the anomalous electroweak Baryon number nonconservation in the Early Universe, Phys. Lett. **155B**, 36 (1985).

[9] S. Rostam Zadeh and S. S. Gousheh, Minimal system including weak sphalerons for investigating the evolution of matter asymmetries and hypermagnetic fields, Phys. Rev. D **99**, 096009 (2019).

[10] A. J. Long, E. Sabancilar, and T. Vachaspati, Leptogenesis and primordial magnetic fields, J. Cosmol. Astropart. Phys. 02 (2014) 036.

[11] V. A. Rubakov and A. N. Tavkhelidze, Stable anomalous states of superdense matter in gauge theories, Phys. Lett. **165B**, 109 (1985).

[12] M. Giovannini and M. E. Shaposhnikov, Primordial hypermagnetic fields and the triangle anomaly, Phys. Rev. D **57**, 2186 (1998).

[13] M. Giovannini and M. E. Shaposhnikov, Primordial Magnetic Fields, Anomalous Matter-Antimatter Fluctuations, and Big Bang Nucleosynthesis, Phys. Rev. Lett. **80**, 22 (1998).
[14] M. Joyce and M. Shaposhnikov, Primordial Magnetic Fields, Right Electrons, and the Abelian Anomaly, Phys. Rev. Lett. **79**, 1193 (1997).
[15] S. Yu. Khlebnikov and M. E. Shaposhnikov, The statistical theory of anomalous Fermion number nonconservation, Nucl. Phys. **B308**, 885 (1988).
[16] S. Rostam Zadeh and S. S. Gousheh, Effects of the $U_Y(1)$ Chern-Simons term and its baryonic contribution on matter asymmetries and hypermagnetic fields, Phys. Rev. D **95**, 056001 (2017).
[17] S. Rostam Zadeh and S. S. Gousheh, Contributions to the $U_Y(1)$ Chern-Simons term and the evolution of Fermionic asymmetries and hypermagnetic fields, Phys. Rev. D **94**, 056013 (2016).
[18] E. Mottola and S. Raby, Baryon number dissipation at finite temperature in the standard model, Phys. Rev. D **42**, 4202 (1990).
[19] P. P. Kronberg, Extragalactic magnetic fields, Rep. Prog. Phys. **57**, 325 (1994).
[20] R. M. Kulsrud and E. G. Zweibel, On the origin of cosmic magnetic fields, Rep. Prog. Phys. **71**, 046901 (2008).
[21] E. R. Harrison, Origin of Magnetic Fields in the Early Universe, Phys. Rev. Lett. **30**, 188 (1973).
[22] J. M. Quashnock, A. Loeb, and D. N. Spergel, Magnetic field generation during the cosmological QCD phase transition, Astrophys. J. Lett. **344**, L49 (1989).
[23] T. W. B. Kibble and A. Vilenkin, Phase equilibration in bubble collisions, Phys. Rev. D **52**, 679 (1995).
[24] G. Sigl, A. V. Olinto, and K. Jedamzik, Primordial magnetic fields from cosmological first order phase transitions, Phys. Rev. D **55**, 4582 (1997).
[25] T. Vachaspati, Magnetic fields from cosmological phase transitions, Phys. Lett. B **265**, 258 (1991).
[26] K. Enqvist and P. Olesen, On primordial magnetic fields of electroweak origin, Phys. Lett. B **319**, 178 (1993).
[27] K. Enqvist and P. Olesen, Ferromagnetic vacuum and galactic magnetic fields, Phys. Lett. B **329**, 195 (1994).
[28] P. Olesen, Inverse cascades and primordial magnetic fields, Phys. Lett. B **398**, 321 (1997).
[29] G. Baym, D. Bodeker, and L. McLerran, Magnetic fields produced by phase transition bubbles in the electroweak phase transition, Phys. Rev. D **53**, 662 (1996).
[30] D. Grasso and H. R. Rubinstein, Magnetic fields in the early universe, Phys. Rep. **348**, 163 (2001).
[31] A. Neronov and I. Vovk, Evidence for strong extragalactic magnetic fields from fermi observations of tev blazars, Science **328**, 73 (2010).
[32] A. Neronov and D. V. Semikoz, Sensitivity of γ-ray telescopes for detection of magnetic fields in the intergalactic medium, Phys. Rev. D **80**, 123012 (2009).
[33] F. Tavecchio, G. Ghisellini, G. Bonnoli, and L. Foschini, Extreme tev blazars and the intergalactic magnetic field, Mon. Not. R. Astron. Soc. **414**, 3566 (2011).
[34] F. Tavecchio, G. Ghisellini, L. Foschini, G. Bonnoli, G. Ghirlanda, and P. Coppi, The intergalactic magnetic field constrained by fermi/large area telescope observations of the tev blazar 1ES 0229+200, Mon. Not. R. Astron. Soc. Lett. **406**, L70 (2010).
[35] A. M. Wolfe, R. A. Jorgenson, T. Robishaw, C. Heiles, and J. X. Prochaska, An 84-μG magnetic field in a galaxy at redshift $z = 0.692$, Nature (London) **455**, 638 (2008).
[36] T. Fujita and K. Kamada, Large-scale magnetic fields can explain the baryon asymmetry of the universe, Phys. Rev. D **93**, 083520 (2016).
[37] M. Giovannini, Anomalous magnetohydrodynamics, Phys. Rev. D **88**, 063536 (2013).
[38] A. J. Long and E. Sabancilar, Chiral charge erasure via thermal fluctuations of magnetic helicity, J. Cosmol. Astropart. Phys. 05 (2016) 029.
[39] M.-C. Chen, S. Ipek, and M. Ratz, Baryogenesis from flavon decays, Phys. Rev. D **100**, 035011 (2019).
[40] C. D. Froggatt and H. B. Nielsen, Hierarchy of quark masses, Cabibbo angles and *CP* violation, Nucl. Phys. **B147**, 277 (1979).
[41] S. Weinberg, Baryon and Lepton Nonconserving Processes, Phys. Rev. Lett. **43**, 1566 (1979).
[42] C. Alvarado, F. Elahi, and N. Raj, Thermal dark matter via the flavon portal, Phys. Rev. D **96**, 075002 (2017).
[43] M. Bauer, T. Schell, and T. Plehn, Hunting the flavon, Phys. Rev. D **94**, 056003 (2016).
[44] A. Banerjee, B. Jain, N. Dalal, and J. Shelton, Tests of neutrino and dark radiation models from galaxy and CMB surveys, J. Cosmol. Astropart. Phys. 01 (2018) 022.
[45] D. J. Eisenstein and W. Hu, Power spectra for cold dark matter and its variants, Astrophys. J. **511**, 5 (1999).
[46] A. J. Cuesta, V. Niro, and L. Verde, Neutrino mass limits: Robust information from the power spectrum of galaxy surveys, Phys. Dark Univ. **13**, 77 (2016).
[47] B. Lillard, M. Ratz, T. M. P. Tait, and S. Trojanowski, The flavor of cosmology, J. Cosmol. Astropart. Phys. 07 (2018) 056.
[48] E. Witten, Branes and the dynamics of QCD, Nucl. Phys. **B507**, 658 (1997).
[49] J. Preskill, S. P. Trivedi, F. Wilczek, and M. B. Wise, Cosmology and broken discrete symmetry, Nucl. Phys. **B363**, 207 (1991).
[50] S. A. Abel, S. Sarkar, and P. L. White, On the cosmological domain wall problem for the minimally extended supersymmetric standard model, Nucl. Phys. **B454**, 663 (1995).
[51] G. Lazarides and Q. Shafi, Axion models with no domain wall problem, Phys. Lett. **115B**, 21 (1982).
[52] T. Hambye, Hidden vector dark matter, J. High Energy Phys. 01 (2009) 028.
[53] G. Arcadi, C. Gross, O. Lebedev, Y. Mambrini, S. Pokorski, and T. Toma, Multicomponent dark matter from gauge symmetry, J. High Energy Phys. 12 (2016) 081.
[54] R. Kitano, H. Murayama, and M. Ratz, Unified origin of baryons and dark matter, Phys. Lett. B **669**, 145 (2008).
[55] V. A. Rubakov and D. S. Gorbunov, *Introduction to the Theory of the Early Universe* (World Scientific, Singapore, 2017).
[56] V. A. Rubakov and M. E. Shaposhnikov, Electroweak baryon number non-conservation in the early universe and in high-energy collisions, Phys. Usp. **39**, 461 (1996).
[57] B. A. Campbell, S. Davidson, J. Ellis, and K. A. Olive, On the baryon, lepton-flavour and right-handed electron

asymmetries of the universe, Phys. Lett. B **297**, 118 (1992).
[58] J. M. Cline, K. Kainulainen, and K. A. Olive, Erasure and Regeneration of the Primordial Baryon Asymmetry by Sphalerons, Phys. Rev. Lett. **71**, 2372 (1993).
[59] J. M. Cline, K. Kainulainen, and K. A. Olive, Protecting the primordial baryon asymmetry from erasure by sphalerons, Phys. Rev. D **49**, 6394 (1994).
[60] J. A. Harvey and M. S. Turner, Cosmological baryon and lepton number in the presence of electroweak fermion number violation, Phys. Rev. D **42**, 3344 (1990).
[61] D. Bodeker and D. Schroder, Equilibration of right-handed electrons, JCAP 1905 (2019) 010.
[62] K. Kamada and A. J. Long, Baryogenesis from decaying magnetic helicity, Phys. Rev. D **94**, 063501 (2016).
[63] A. Vilenkin, Equilibrium parity violating current in a magnetic field, Phys. Rev. D **22**, 3080 (1980).
[64] M. Laine, Real-time chern-simons term for hypermagnetic fields, J. High Energy Phys. 10 (2005) 056.
[65] T. Appelquist and R. D. Pisarski, High-temperature Yang-Mills theories and three-dimensional quantum chromodynamics, Phys. Rev. D **23**, 2305 (1981).
[66] K. Kajantie, M. Laine, K. Rummukainen, and M. Shaposhnikov, Generic rules for high temperature dimensional reduction and their application to the standard model, Nucl. Phys. **B458**, 90 (1996).
[67] A. Avkhadiev and A. V. Sadofyev, Chiral vortical effect for bosons, Phys. Rev. D **96**, 045015 (2017).
[68] V. P. Kirilin and A. V. Sadofyev, Anomalous transport and generalized axial charge, Phys. Rev. D **96**, 016019 (2017).
[69] K. Fukushima, D. E. Kharzeev, and H. J. Warringa, The chiral magnetic effect, Phys. Rev. D **78**, 074033 (2008).
[70] D. E. Kharzeev, J. Liao, S. A. Voloshin, and G. Wang, Chiral magnetic and vortical effects in high-energy nuclear collisions—A status report, Prog. Part. Nucl. Phys. **88**, 1 (2016).
[71] Y.-C. Liu and X.-G. Huang, Anomalous chiral transports and spin polarization in heavy-ion collisions, Nucl. Sci. Tech. **31**, 56 (2020).
[72] S. Abbaslu, S. Rostam Zadeh, and S. S. Gousheh, Contribution of the chiral vortical effect to the evolution of the hypermagnetic field and the matter-antimatter asymmetry in the early Universe, Phys. Rev. D **100**, 116022 (2019).
[73] R. Lüst and A. Schlüter, Kraftfreie magnetfelder. Mit 4 textabbildungen, Z. Astrophys. **34**, 263 (1954).
[74] S. Chandrasekhar and L. Woltjer, On force-free magnetic fields, Natl. Acad. Sci. lett. **44**, 285 (1958).
[75] S. Chandrasekhar and P. C. Kendall, On force-free magnetic fields, Astrophys. J. **126**, 457 (1957).
[76] A. Boyarsky, J. Frohlich, and O. Ruchayskiy, Self-Consistent Evolution of Magnetic Fields and Chiral Asymmetry in the Early Universe, Phys. Rev. Lett. **108**, 031301 (2012).
[77] A. Boyarsky, J. Frohlich, and O. Ruchayskiy, Magnetohydrodynamics of chiral relativistic fluids, Phys. Rev. D **92**, 043004 (2015).
[78] M. Dvornikov and V. B. Semikoz, Leptogenesis via hypermagnetic fields and baryon asymmetry, J. Cosmol. Astropart. Phys. 02 (2012) 040; Erratum, J. Cosmol. Astropart. Phys. 08 (2012) E01.
[79] M. Giovannini, Hypermagnetic knots, Chern-Simons waves and the baryon asymmetry, Phys. Rev. D **61**, 063502 (2000).
[80] W. Chen, B. D. Chowdhury, F. Ferrer, H. Tashiro, and T. Vachaspati, Intergalactic magnetic field spectra from diffuse gamma rays, Mon. Not. R. Astron. Soc. **450**, 3371 (2015).
[81] A. Saveliev, K. Jedamzik, and G. Sigl, Evolution of helical cosmic magnetic fields as predicted by magnetohydrodynamic closure theory, Phys. Rev. D **87**, 123001 (2013).
[82] H. Tashiro, T. Vachaspati, and A. Vilenkin, Chiral effects and cosmic magnetic fields, Phys. Rev. D **86**, 105033 (2012).
[83] V. B. Semikoz and A. Yu. Smirnov, Leptogenesis in the symmetric phase of the early universe: Baryon asymmetry and hypermagnetic helicity evolution, J. Exp. Theor. Phys. **120**, 217 (2015).
[84] P. Pavlović, N. Leite, and G. Sigl, Chiral magnetohydrodynamic turbulence, Phys. Rev. D **96**, 023504 (2017).
[85] S. Abbaslu, S. Rostam Zadeh, and S. S. Gousheh, The generation of matter-antimatter asymmetries and hypermagnetic fields by the chiral vortical effect of transient fluctuations, arXiv:2001.03499.
[86] O. D. Miranda, M. Opher, and R. Opher, Seed magnetic fields generated by primordial supernova explosions, Mon. Not. R. Astron. Soc. **301**, 547 (1998).
[87] C. G. Tsagas, P. K. S. Dunsby, and M. Marklund, Gravitational wave amplification of seed magnetic fields, Phys. Lett. B **561**, 17 (2003).
[88] K. Enqvist, A. Jokinen, and A. Mazumdar, Seed perturbations for primordial magnetic fields from minimally supersymmetric standard model flat directions, J. Cosmol. Astropart. Phys. 11 (2004) 001.
[89] A. Ashoorioon and R. B. Mann, Generation of cosmological seed magnetic fields from inflation with cutoff, Phys. Rev. D **71**, 103509 (2005).
[90] H. Hanayama, K. Takahashi, K. Kotake, M. Oguri, K. Ichiki, and H. Ohno, Biermann mechanism in primordial supernova remnant and seed magnetic fields, Astrophys. J. **633**, 941 (2005).
[91] K. E. Kunze, Primordial magnetic seed fields from extra dimensions, Phys. Lett. B **623**, 1 (2005).
[92] V. B. Semikoz and J. W. F. Valle, Lepton asymmetries and the growth of cosmological seed magnetic fields, J. High Energy Phys. 03 (2008) 067.
[93] H. Hanayama, K. Takahashi, and K. Tomisaka, Generation of seed magnetic fields in primordial supernova remnants, arXiv:0912.2686.
[94] K. Subramanian, From primordial seed magnetic fields to the galactic dynamo, Galaxies **7**, 47 (2019).